## Title

Three-Dimensional Flow and Thermal Structure in Glass Melting Furnaces. Part II: Effect of Batch and Bubbles



## Journal

Glass Science and Technology, 75(3)

## Authors

Pilon, Laurent
Zhao, Guochang
Viskanta, Raymond

## Publication Date

2002

Peer reviewed

# Three-Dimensional Flow and Thermal Structures in Glass Melting Furnaces. Part II: Effect of Batch and Bubbles. Glass Science and Technology, Vol. 75, No.3 pp. 115-124.

Laurent Pilon, Guochang Zhao, and Raymond Viskanta

Heat Transfer Laboratory
School of Mechanical Engineering
Purdue University
West Lafayette, IN 47907, USA

Phone: (765)-494-5632
Fax: (765)-494-0539
E-mail: viskanta@ecn.purdue.edu

January 15, 2006

# ABSTRACT

This paper is the second part (Part II) of a parametric study of the flow and thermal structure in glass melting furnaces with a throat. The effects of the following parameters are discussed: (i) the batch velocity, (ii) the melting temperature, (iii) the submerged depth of the batch, (iv) the wall heat losses, and (v) the thickness of glass melt containing gas bubbles under the batch. The study indicates that the partially submerged batch and heat losses through the refractories have a strong impact on both the longitudinal and spanwise flow patterns of the molten glass. These physical phenomena must be accounted for if one wants to realistically simulate the natural convection circulation of the molten glass in the bath.


# NOMENCLATURE

| | |
|---|---|
| $c$ | Specific heat |
| $\Delta H_{melt}$ | Total enthalpy of melting of the batch |
| $g$ | Specific gravity |
| $h$ | Depth within the glass melt |
| $k$ | Thermal conductivity |
| $L_b$ | Length of the batch blanket |
| $L_{max}$ | Longitudinal location of the maximum heat flux |
| $L_0$ | Longitudinal location of the zero heat flux |
| $\dot{m}_b$ | Batch mass flow rate |
| $\dot{m}_{melt}$ | Glass mass flow rate at the throat |
| $q''$ | Heat flux |
| $q''_0$ | Heat flux at the back wall (x = 0 m) |
| $Q'_{melt \rightarrow batch}$ | Heat transfer rate from the glass melt to the batch per unit length of batch |
| $T$ | Temperature |
| $u$ | Velocity vector in the x-direction |
| $v$ | Velocity vector in the y-direction |
| $w$ | Velocity vector in the z-direction |
| $W$ | Glass tank width |
| $x$ | Longitudinal location (see Figure 1) |
| $y$ | Spanwise location (see Figure 1) |
| $z$ | Local depth within the glass melt (see Figure 1) |
| **Greek symbols** | |
| $\alpha$ | Thermal diffusion coefficient |
| $\rho$ | Density |
| $\mu$ | Dynamic viscosity |
| $\phi$ | Local volumetric gas fraction |
| **Subscripts** | |
| $b$ | Refers to the batch |
| $bubbles$ | Refers to the depth under the batch where bubbles are present |
| $g$ | Refers to gases contained in the bubbles |
| $m$ | Refers to the mixture of the molten glass and the gases bubbles |
| $melt$ | Refers to the melting of the batch |
| $max$ | Refers to the value at x = $L_{max}$ |
| $sub$ | Refers to the submerged part of the batch |
| $\infty$ | Refers to the molten glass |

# INTRODUCTION

This is a second part of a study concerned with the three-dimensional natural circulation in glass melting furnaces with a throat. The first part of the paper presents a literature review of the topic and discusses the mathematical model employed in the numerical simulations [1]. In brief, the complex processes of the

transformation of the raw batch into glass melt is not modeled, nor are the flow, chemical reactions, and temperature fields in the combustion space. The basic features of the mathematical model and the numerical method employed to compute the flow and temperature fields in the glass melt are detailed elsewhere [2, 3] and need not to be repeated here. Note that for the first time a consistent set of thermophysical properties of soda-lime solicate glass of composition 74 $SiO_2$-16 $Na_2O$-10 CaO (mol.%) has been collected for use as input parameters in the numerical simulations.

The first part of the study is aimed at evaluating the capability of the furnace operators to control the glass flow and thermal structures by adjusting the fuel firing in the combustion space. The heat flux distribution resulting from combustion of fossil fuel and the net flux incident on the surface of the batch and of the molten glass is assumed to be uniform across the tank width and to have the longitudinal profile as shown in Figure 2 where the parameters $q''_{max}$ and $q''_0$ are the maximum heat flux, and the heat flux at the back wall (x=0 m), respectively. The distances from the back wall to the location of the maximum heat flux and to the location where the heat flux vanishes are denoted by $L_{max}$ and $L_0$, respectively. Particular attention was paid to the effects of (i) the uniformity of the net heat flux from the combustion space incident on the glass melt, (ii) the location of the zero heat flux $L_0$, (iii) the location of the maximum heat flux $L_{max}$, (iv) the presence of a foam layer, and (v) the shape of the heat flux in the spanwise direction. In all the simulations, the total heat input was held constant and equal to 8.3 MW, and the qualitative analysis presented in Part I [1] leads to the following conclusions:

1. A heat flux gradient in the x-direction is required to generate two recirculation loops in the longitudinal direction.

2. A steep heat flux gradient in the refining part of the tank increases significantly the extent of the second recirculation loop. In the present analysis, the steepest heat flux gradient is obtained by modifying the location of the zero heat flux.

3. The change of the heat flux distribution has no appreciable effect on the flow pattern under the batch blanket. Sixteen roll cells develop under the entire length of the batch, but the cells disappear where the glass is free of batch.

4. The negative heat flux at the glass melt surface causes two cells to form in the lateral direction at the surface of the glass melt and close to the front wall.

In Part I [1], the batch blanket was assumed to be on top of the molten glass surface. In reality, part of the batch is submerged into the molten glass, thus effectively reducing the flow area under the batch. Similarly, the presence of gas bubbles under the batch generated during the melting of the batch may affect the velocity and the temperature fields of the molten glass since bubbles change the thermophysical properties of the fluid. Finally, the rheology of the batch is not fully understood, and simplifying assumptions are required in order to predict the batch velocity.

This part (Part II) of the paper presents a systematic parametric study of the effects of the velocity, the melting temperature, and the submerged part of the batch into the molten glass, as well as the effects of the bubbles under the batch on the flow and temperature fields.

# RESULTS AND DISCUSSION

## Glass Tank and Parameters

The tank considered was 15.85 m long, 7.315 m wide, and 1.03 m deep (see Figure 1). The molten glass exits the tank through a throat located at the bottom and in the middle of the front wall and having a cross-sectional area of (0.386×0.802) $m^2$.

The raw batch materials produce a glass melt having composition of 74 $SiO_2$-16 $Na_2O$-10 CaO (mol.%). The batch is introduced into the tank at a rate $\dot{m}_b$ of 356 ton/day (or 4.12 kg/s) in the form of a 6.5 m long and loose blanket covering the entire width of the tank. The length of the batch blanket $L_b$ (=6.5 m) was chosen arbitrarily based on the two-dimensional study by Lim *et al.* [4] who showed that the batch blanket should cover between 25 to 40% of the glass surface for an optimum melting rate. The batch enters the tank at a temperature of 320 K. Since about 200 kg of gases are produced per ton of batch introduced [5],

the corresponding glass pull (production) rate $\dot{m}_{pull}$ is 297 tons/day (or 3.437 kg/s) of molten glass. The melting of raw batch materials is a complex physicochemical process which involves a large number of chemical reactions and phase transformations occurring over the wide temperature range from 1000 to 1500 K [6]. Thus, the melting of the batch cannot be treated has a change of phase (from solid to liquid) at a discrete temperature. In order to model the melting process, a constant temperature (called melting temperature and noted $T_{melt}$) was imposed at the batch/glass melt interface corresponding to the minimum temperature at which a clear glass is obtained. Madivate [7] has reported experimental data for the energy required to bring the batch from room temperature to clear molten glass $\Delta H_{melt}$. The value of 2200 kJ/kg of glass of compositions similar to that of interest in the present work was retained for $\Delta H_{melt}$ for soda-lime silicate glass having composition 74 $SiO_2$-16 $Na_2O$-10 CaO (mol.%) and a melting temperature of 1450 K.

The heat flux distribution is maintained the same for all the simulations:

1. The location of the maximum heat flux $L_{max}$ (see Figure 2) was chosen 1 m ahead of the batch tip (i.e., $L_{max}$=7.5 m) in order to create a hot spring forcing the glass melt to circulate in two recirculation loops.

2. The maximum heat flux $q''_{max}$ is estimated by writing the energy balance equation for the batch blanket of length $L_b = 6.5$ m:
$$Q'_{melt\rightarrow batch} L_b + \int_0^{L_b} q''(x) W \mathrm{d}x = \dot{m}_{melt} \Delta H_{melt} \tag{1}$$
where $Q'_{melt\rightarrow batch}$ is the heat transfer rate from the glass melt to the batch per unit length of batch. The heat flux from the combustion space to the surface of the glass melt is $q''(x)$, $W$ is the width of the tank (=7.315 m), $\Delta H_{melt}$ is the enthalpy per unit mass of molten glass required to obtain clear glass at the melting temperature $T_{melt}$ from raw batch at 320 K. Finally, $\dot{m}_{melt}$ is the pull rate, i.e., the total mass of glass leaving the furnace through the throat per unit of time. The determination of $Q'_{melt\rightarrow batch}$ requires several interations. However, we found that the value does not change significantly from one simulation to the next. In the present study, a good approximate value for $Q'_{melt\rightarrow batch}$ is $3 \times 10^6$ W/m.

3. The zero heat flux is located 2 m away from the front wall, i.e., $L_0 = 13.84$ m.

In summary, all the simulations of Part II use the same net heat flux distribution from the combustion space to the glass surface that is characterized by the following parameters:

$$q''_{max} = 133.92 \text{ kW/m}^2 \qquad \textit{and} \qquad q''_0 = q_{max}/2 \tag{2}$$
$$L_{max} = 7.5 \text{ m} \qquad \textit{and} \qquad L_0 = 13.84 \text{ m} \tag{3}$$

The total energy input rate from the combustion space to the glass melt is calculated by integrating the heat flux distribution over the entire surface of the tank. The resulting total heat input rate from the combustion space is equal to 8.3 MW and is kept the same for all the simulations. Similarly, the pull rate $\dot{m}_{melt}$ remains constant and equals 3.347 kg/s.

The same baseline case as Part I is used and the reader is refered to Ref. [1] for a complete description of the parameters and of the results. The effects of several operating parameters on the glass flow structure in the tank are studied, in particular:

(a) *The batch axial velocity $u_b$*

(b) *The melting temperature $T_{melt}$*

(c) *The flow reduction under the batch due to*

  (i) the sinking of the batch with and without heat losses through the side walls

  (ii) The presence of a layer of gas bubbles under the batch.

Table 1 summarizes the conditions prescribed in the different simulations presented in the following sections.

## Effect of Batch Axial Velocity $u_b$

Depending on the charging method, the batch may assume different shape (form) and velocities. As a first approximation, we assumed that the batch blanket can only have an axial velocity $u_b$. Figure 3 compares the flow and temperature fields for a batch velocity equals to 0.0 cm/s and 0.2 cm/s (baseline case). The effects of the batch velocity seem to be limited to the regions under the batch and near the front wall. Indeed, a cell develops across the width under the batch when the batch has a non-zero velocity in the x-direction. This is due to the shear between the batch and the glass melt. Moreover, a slight change in the isotherms can be observed near the front wall for isotherm 1600 K. However, the batch velocity does not affect significantly the temperature and the velocity fields of the glass melt in other parts of the tank. Ungan and Viskanta [8] have found that the batch velocity affects the local temperature and velocity fields near the batch/glass melt interface. However, they assumed that there was no pull in the tank studied.

## Effect of the Melting Temperature $T_{melt}$

As discussed by Laimbock [9], a clear glass is obtained at 1473 K from fine silica powder, while for coarse silica powder it is produced at 1673 K. Even though the melting of the batch is not modeled in the present work, changes in the size of the sand grains can be simulated by changing the temperature at which a clear glass in obtained. The melting temperatures was changed while the enthalpy of melting was maintained constant in order to keep the batch length unchanged. Indeed, the batch coverage is believed to strongly affect the flow pattern of the molten glass in the bath and it is important to keep the batch length constant. Moreover, the enthalpy $\Delta H_{melt}$ varies slightly from around 2175 kJ/kg of glass at 1350 K to about 2300 kJ/kg of glass at 1550 K.

Figures 4 and 5 compare the flow and the temperature fields at the centerline for three different melting temperatures (1350 K, 1450 K, and 1550 K). One can observe that as the melting temperature decreases, an additional cell develops under the batch in the spanwise direction. The axial velocity of the batch combined with the exponential increase of the glass melt viscosity with the decreasing temperature are responsible for the large shear stress at the batch/glass melt interface that propagates deeper in the glass melt and generates a cell that expands across the tank in the spanwise direction.

The most significant effects of the melting temperature are the steeper temperature gradients in the z-direction obtained for low melting temperatures. Note also that the intensity of the glass circulation glass in the entire glass bath increase significantly with an increase in the melting temperature due to a decrease in the glass melt viscosity. However, beyond the batch tip (i.e., $x > L_b$), the net glass flow rate through any given cross-section perpendicular to the x-direction is not affected by the melting temperature and is equal to the glass pull rate $\dot{m}_{pull}$ at the throat. For example, at x = 7.5 m and for a melting temperature of 1450 K and 1550 K, the forward mass flow rate equals 10.5 kg/s and 12.4 kg/s, respectively, the backward mass flow rate equals 7.1 kg/s and 9.0 kg/s, respectively, and the net mass flow rate is identical in both cases and is equal to the glass pull rate of 3.437 kg/s.

In addition to these effects, the flow field is not qualitatively modified: the number of cells in the spanwise direction and the flow patterns in the longitudinal direction are similar to those observed in the baseline case (see Part I [1]). Moreover, even though the temperature gradients in the vertical direction are significantly affected by the melting temperature, the maximum surface temperatures do not change significantly.

## Effect of the Flow Reduction Under the Batch

### Partially Submerged Batch

The batch raw material is lighter than the molten glass and float at the surface of the glass melt. A significant part of the batch is submerged under the glass free surface. In simulating the submerged batch one needs to know its density, its specific heat, and its effective conductivity. They were obtained from the literature [10]:

$$\rho_b = 1400 \quad kg/m^3 \tag{4}$$

$$c_b = 1.1 \times 10^3 \quad J/kgK \tag{5}$$

$$k_b = 0.2465 + 1.88 \times 10^{-4}T + 1.69 \times 10^{-7}T^2 \quad W/mK \tag{6}$$

The momentum equation for a batch blanket of uniform thickness at rest projected onto the vertical axis indicates that the ratio of the submerged batch depth to the total batch thickness $h_{sub}/h_b$ equals the ratio of the batch density to the glass melt density $\rho_b/\rho$. For the batch considered, 11.2 cm ($=h_{sub}$) of the 20 cm thick batch blanket is submerged. The fact that the batch is partially submerged in the molten glass can be modeled by imposing the thermophysical properties of the batch given by Equations (4) through (6) and by forcing the viscosity to be very large in an arbitrary region of the computational domain located under the batch blanket. In reality, the thickness of the batch blanket decreases as the batch is being pushed and melts due to the heating from the combustion space. In the present work, however, we assumed as a first order approximation that the part of the batch submerged was of uniform thickness $h_{sub}$ across the tank width and from the back wall to the tip of the batch blanket. Two simulations were performed: (i) one accounting for the heat losses through the refractories, and (ii) the other assuming that the walls were adiabatic. In both the submerged batch depth $h_{sub}$ was equal to 10.4 cm corresponding to four (4) computational grid cells.

Figure 6 compares the flow patterns in the spanwise direction for these two cases at different cross-sections of the tank. One can see that the effect of the cooling of the walls has a significant impact on the flow patterns. In the case of adiabatic side walls, a very unstructured flow pattern occurs under the batch and disappears when heat losses to the surroundings are accounted for. For example, no cells are observed near the bottom of the tank in the adiabatic case. This indicates that the cooling of the bottom and of the side walls are responsible for the cell formation at the bottom of the tank when batch is absent on the glass surface. Moreover, the cells forming close to the front wall develop whether the walls are adiabatic or not. Therefore, the negative heat flux (i.e., heat loss from the glass surface) at the end of the furnace is mainly responsible for the two cells forming near the surface close to the front wall. Finally, given the importance of the heat losses through the refractories and the formation of the cells at the corners where two or three walls are joined, modeling of the heat conduction using a one-dimensional treatment may not be satisfactory and multidimensional effects should be accounted for. In summary, the effects of the heat losses through the refractory walls dominate the three dimensional natural convection circulation of the molten glass. Note that the effects of the heat losses were assessed when the batch was submerged to avoid the computational complications encountered by Lim *et al.* [11] who observed the possible unsteady periodic and even chaotic behavior of the flow field requiring a unsteady mathematical formulation. Such an unsteady behaviors does not seem to prevail when the sinking of the batch and/or the heat losses are accounted for. To further assess the effects the sinking of the batch an additional value of the thicknesses $h_{sub}$ was considered ($h_{sub} = 21$ cm corresponding to 6 grid cells). The results are discussed in the next section.

**Effect of the Bubbles Under the Batch**

Laboratory experiments showed that a large number of bubbles are present under the batch due to the gas generation taking place during the batch melting process [12]. The presence of the bubbles under the batch affects the thermophysical properties of the fluid. It forces the density of the fluid mixture to decrease and its viscosity to increase [13]. Then, in the region containing bubbles, the density of the melt should be substituted by that of the mixture $\rho_m$ expressed as [14]

$$\rho_m = \rho_g \phi + \rho_\infty (1 - \phi) \tag{7}$$

where $\phi$ is the local gas void fraction and $\rho_g$ the density of the gas contained in the bubbles. On the other hand, Ishii [13] recommended the following expression for the viscosity of the mixture $\mu_m$ for a bubbly flow

$$\frac{\mu_m}{\mu_\infty} = (1 - \phi)^{-1} \tag{8}$$

Equation (8) indicates that the viscosity of the mixture increases as the gas void fraction increases due to the resistance of the bubbles to the deformation of the flow field caused by their presence. The bubbles were assumed to occupy a 10.4 cm deep region of the glass melt under the batch. A volumetric void fraction $\phi$ of

0.2 was arbitrarily chosen as a maximum value for the gas void fraction. Note that, as a first order approximation, the thermophysical properties of the glass melt containing bubbles was assumed to be identical to that without bubbles.

The cells present under the batch are due to Rayleigh-Taylor instabilities caused by the fact that the glass melt at the batch/glass melt interface is heavier than that present at the bottom of the tank. A priori, one can predict that reducing the density of the glass melt immediately under the batch (i.e., at the top of the glass melt) due to the presence of the bubbles would significantly affect the cells and even eliminate them when the density of the two-phase mixture located under the batch becomes smaller than that of the molten glass phase at the bottom of the tank. As one can see in figures **??** and 9, the thermal structure in the longitudinal direction and the streamlines under the batch for the baseline case (figure **??**a) are similar to those when bubbles are present under the batch (figure **??**e). Therefore, the effects of the presence of bubbles on the density and the viscosity of the two-phase mixture does not alter significantly the thermal and flow structure of the molten glass. However, their effects on the thermal conductivity and specific heat of the two-phase mixture has not been accounted for and it is beyond the scope of the present study to model and simulate such effects.

Figures 9 and 10 compare the effects of the partially submerged batch and of the presence of the bubbles on the flow pattern and thermal structure under the batch. As already mentioned, the results indicate that the submerged batch strongly affects the Rayleigh-Benard cells under the batch. The number of cells decreases from 16 when the sinking of the batch is neglected (i.e., $h_{sub}$=0 cm) to only two when the batch is submerged under the glass free surface. In figure 10, one can observe the isotherms under the batch 3.5 m from the back wall. It is interesting to note that the 16 cells developing under the batch (see figure 9a) in the baseline case go in pairs. In other words, each one of the eight (8) 1510 K isotherms in figure 10a contains two (2) cells in which the fluid cicrculates in opposite directions (clockwise and counterclockwise). The largest isotherm loops are located between the midplane and the wall and surrounded by two cells. In contrast, when the batch is submerged, the isotherm loops that can be plotted are much smaller, and the largest ones are located along the sidewalls. Even though other isotherm loops are present their driving force is insufficient to form Rayleigh-Benard cells and only two Rayleigh-Benard cells are actually observed along the sidewalls where the largest isotherm loops are formed. Therefore, any other cells forming away from the side walls, even though observed in experimental model simulations [15], are not likely to occur in actual melting furnace where the batch is always partially submerged. Note also that the presence of gas bubbles does not affect the thermal structure of the molten glass under the batch.

Simulations were also performed by using the effective conductivity of the glass melt in the region where the batch is submerged instead of that of the batch. They indicate a strong effect of the thermal conductivity of the batch on the thermal structure of the glass melt. When the batch thermal conductivity is used, the temperature gradients in the z-direction change drastically as observed in figure **??**. The batch introduces a greater thermal resistance to heat transfer than a glass melt layer of the same thickness. However, the streamlines under the batch in the spanwise direction are not afffected as shown in figure 9. Therefore, the temperature gradients in the z-direction have no influence on the cells forming under the batch. Instead, the cells are due to the gradients of temperature in the y-direction. The latter is due to the cooling of the side walls as suggested by Ungan and Viskanta [16].

Furthermore, the flow patterns in the longitudinal direction from the batch tip to the front wall in the presence of bubbles or when the batch is submerged are very similar to those of the baseline case shown in Part I [1] and need not to be repeated. In all the cases, the ideal flow pattern presented in figure 11 is not observed but that presented in figure 12 seems to represent the simulation results. Note also that the largest heat transfer rate from the glass melt to the batch was found for adiabatic walls since the glass temperature was larger for this case and that the cells under the batch can increase the heat transfer from the glass melt to the batch by up to 20%.

Finally, visual observations of the wear of the refractories in operating glass melting furnaces after a production campaign confirm the presence of the two cells close to the side walls under the batch and that of two cells forming close at the front wall due to the combined effects of the cooling of the side walls, of the front wall, and of the glass surface to the combustion space [17]. Consequently, the sinking of the batch below the glass surface and the heat losses through the walls should be carefully accounted for if one aims to obtain realistic predictions of the flow patterns in operating glass melting furnaces.

# CONCLUSIONS

This paper presents a parametric study of the flow patterns in glass melting furnaces with a throat. In particular, the effects of the following parameters are discussed: (i) the batch velocity $u_b$, (ii) the melting temperature $T_{melt}$, (iii) the submerged depth of the batch $h_{sub}$, (iv) the wall heat losses, and (v) the thickness of bubble layer under the batch $h_{bubbles}$. The qualitative analysis presented leads to the following conclusions:

1. The flow pattern observed by Zhiqiang and Zhihao [18] in the longitudinal direction and represented in Figure 12 is confirmed. A part of the pull moves directly from under the batch to the throat. Such a flow pattern tends to deteriorate the glass quality since unmelted sand grains and gas bubbles generated under the batch may not have sufficiently long residence time to melt or rise to the surface and may leave the tank through the throat.

2. The flow pattern does not change significantly with the melting temperature. As the melting temperature decreases, a cell develops in the spanwise direction of the tank close to the back wall where the batch is introduced with a non-zero velocity. The exponential increase of the viscosity as the temperature decreases causes the shear stress between the glass melt and the batch to increase and is responsible for the cell formation. Such an effect is localized and does not extend to other regions of the tank. Finally, as the melting temperature decreases, the temperature gradient within the glass melt in the vertical direction are larger as well as the magnitude of the velocity vectors.

3. Neither the batch velocity nor the presence of the bubbles under the batch seem to significantly affect the flow pattern. The sixteen cells observed under the batch when the sinking of the batch is neglected, i.e., $h_{sub}$ =0 cm, are replaced by only two cells when the batch is submerged.

4. The heat losses through the refractories have a strong impact on the flow pattern of the molten glass. In absence of heat losses through the walls, an unstructured flow pattern can be observed in the spanwise direction, but it vanishes when the heat losses are accounted for. Therefore, the heat losses through the walls control in part the spanwise flow structure and must be accounted for if one wants to realistically simulate the natural convection circulation of the molten glass in the bath.

5. Given the importance of the heat losses through the refractory walls on the flow structure and the fact that cells form preferentially at the intersection of the walls, a more refined heat conduction model through the refractories may need to be developed to account for the multidimensional effects and to obtain a realistic predictions of the flow and thermal fields of the glass melt.

# References


[1] L. Pilon, G. Zhao, and R. Viskanta, "Three-dimensional flow and thermal structures in glass melting furnaces. Part I. effects of the heat flux distribution", *Glass Science and Technology*, vol. 75, no. 2, pp. 55–68, 2002.

[2] A. Ungan and R. Viskanta, "Three-dimensional numerical modeling of circulation and heat transfer in a glass melting tank. Part. 1 mathematical formulation", *Glastechnische Berichte*, vol. 60, No.3, pp. 71–78, 1987.

[3] R. Viskanta, "Review of three-dimensional mathematical modeling of glass melting", *Journal of Non-Crystalline Solids*, vol. 177, pp. 347–362, 1994.

[4] K-O Lim, T-H Song, and K-S Lee, "Pattern of natural convection driven by the free surface temperature distribution in a glass melting furnace", *Glass Technology*, vol. 39, pp. 27–31, 1998.

[5] C. Madivate, F. Müller, and W. Wilsmann, "Calculation of the theoretical energy requirement for melting technical silicate glasses", *Journal of the American Ceramic Society*, vol. 81, pp. 3300–3306, 1998.

[6] A. Ungan and R. Viskanta, "Melting behavior of continuously charged loose batch blankets in glass melting furnaces", *Glastechnische Berichte*, vol. 59, No.10, pp. 279–291, 1986.

[7] C. Madivate, "Calculation of the theoretical energy requirement for melting technical silicate glasses", *Journal of the American Ceramic Society*, vol. 81, pp. 3300–3306, 1998.

[8] A. Ungan and R. Viskanta, "Three-dimensional numerical modeling of circulation and heat transfer in a glass melting tank. Part. 2 sample simulations", *Glastechnische Berichte*, vol. 60, No.4, pp. 115–124, 1987.

[9] P. R. Laimbock, *Foaming of glass melts*, PhD thesis, Technical University of Eindhoven, Eindhoven, The Netherlands, 1998.

[10] R. Viskanta and X. Wu, "Effect of gas percolation on melting of glass batch", *Journal of the American Ceramic Society*, vol. 67, No. 5, pp. 376–380, 1984.

[11] K-O Lim, K-S Lee, and T-H Song, "Primary and secondary instabilities in a glass-melting surface", *Numerical Heat Transfer, Part A*, vol. 36, pp. 309–325, 1999.

[12] S. Kawachi and Y. Kawase, "Evaluation of bubble removing performance in a TV glass furnace. Part 2. verification using real furnace data", *Glastechnische Berichte*, vol. 71, No.5, pp. 111–119, 1998.

[13] M. Ishii and T. C. Chawla, "Local drag laws in dispersed two-pahse flow", ANL-79-105, NUREG/CR-1230, 1979.

[14] G. B. Wallis, *One-dimensional two-phase flow*, McGraw-Hill, New York, 1969.

[15] N. W. E. Curlet, K. J. Won, L. A. Clomberg Jr., and A. F. Sarofim, "Experimental and mathematical modeling of three-dimensional natural convection in an enclosure", *AIChE Journal*, pp. 249–257, 30, No. 2.

[16] A. Ungan and R. Viskanta, "Identification of the structure of the three dimensional thermal flow in an idling container glass melter", *Glass Technology*, vol. 28, No. 6, pp. 252–260, 1987.

[17] C. Jian, "Owens Corning Company", Personal communication, March 2001.

[18] Y. Zhiqiang and Z. Zhihao, "Basic flow pattern and its variation in different types of glass tank furnaces", *Glastechnische Berichte*, vol. 70, pp. 165–172, 1997.

## Figure Captions

**Figure 1.** *Schematic of the modelled glass melting tank and its system of coordinates.*

**Figure 2.** *Heat flux distribution used as the boundary condition at the glass melt/combustion space interface.*

**Figure 3.** *Effect of the batch velocity on (a) the velocity field, (b) the streamlines at the tank centerline for* $u_{batch}$ *=0.0 cm/s and 0.2 cm/s (baseline case).*

**Figure 4.** *Effect of* $T_{melt}$ *on the streamlines at the centerline for (a)* $T_{melt}$ *= 1350 K, (b)* $T_{melt}$ *= 1450 K, (c)* $T_{melt}$ *= 1550 K.*

**Figure 5.** *Effect of* $T_{melt}$ *on the temperature field at the centerline for (a)* $T_{melt}$ *= 1350 K, (b)* $T_{melt}$ *= 1450 K, (c)* $T_{melt}$ *= 1550 K.*

**Figure 6.** *Comparison of the streamlines in the spanwise direction at location (a) x = 3.5 m, (b) x = 7 m, and (c) x = 15 m for a 10.4 cm submerged batch with (left) and without (right) heat losses through the side walls.*

**Figure 7.** *Effect of the flow reduction under the batch on the streamlines at the centerline for (a)* $h_{sub}$*=0 m, (b)* $h_{sub}$*=0.104 m, (c)* $h_{sub}$*=0.21 m, and (d)* $h_{bubbles}$*=0.104 m.*

**Figure 8.** *Effect of the flow reduction under the batch on the temperature field at the centerline for (a)* $h_{sub}$*=0 m, (b)* $h_{sub}$*=0.104 m, (c)* $h_{sub}$*=0.21 m, and (d)* $h_{bubbles}$*=0.104 m.*

**Figure 9.** *Effect of the flow reduction under the batch on the streamlines for (a)* $h_{sub}$*=0 m, (b)* $h_{sub}$*=0.104 m, (c)* $h_{sub}$*=0.21 m, (d)* $h_{bubbles}$*=0.104 m, and (e) adiabatic walls.*

**Figure 10.** *Effect of the flow reduction under the batch on the temperature field for (a)* $h_{sub}$*=0 m, (b)* $h_{sub}$*=0.104 m, (c)* $h_{sub}$*=0.21 m, and (d)* $h_{bubbles}$*=0.104 m.*

**Figure 11.** *Schematic of the ideal flow pattern furnaces with a throat.*

**Figure 12.** *Schematic of the flow pattern observed by zhiqiang and Zhihao (1997) in furnaces with a throat.*

## Table Captions

**Table 1.** *Summary of the parameters used in the three-dimensional simulation.*

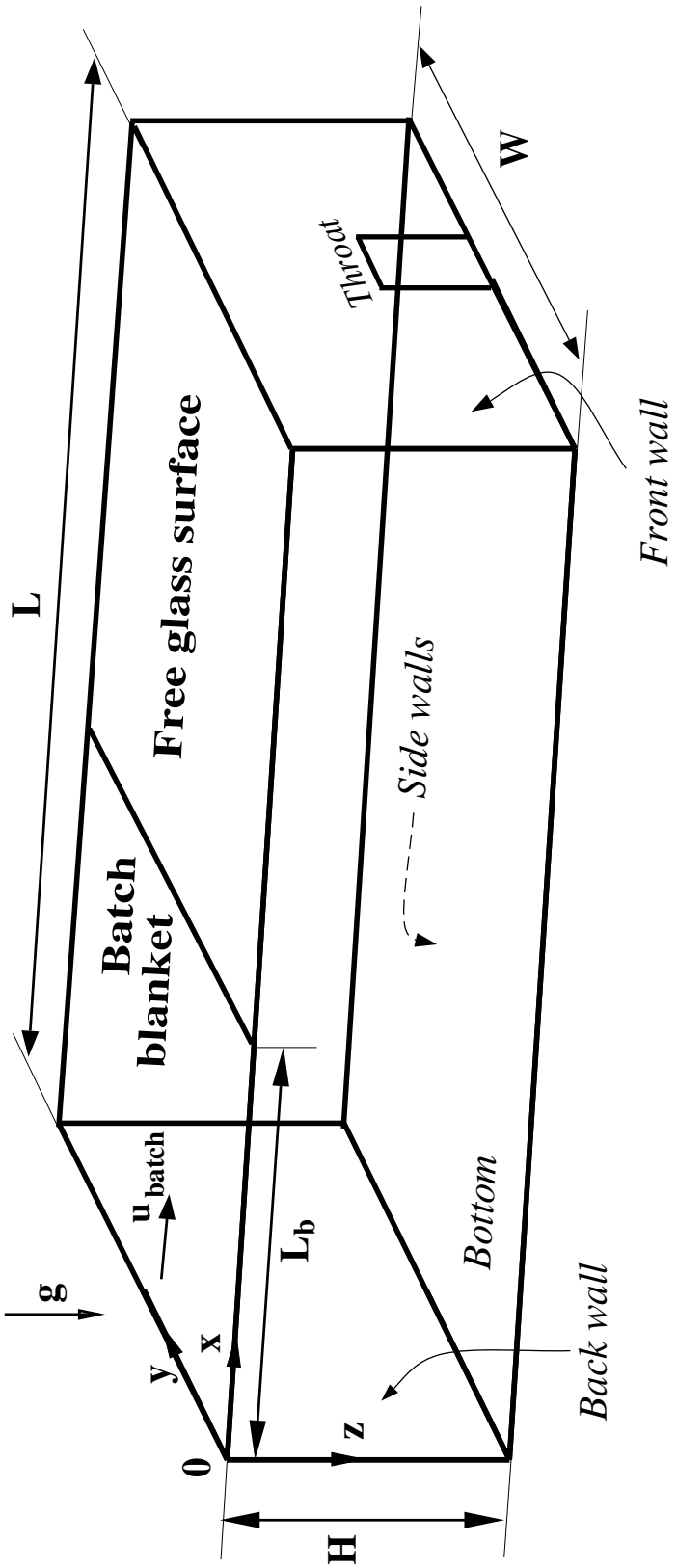


Figure 1: *Schematic of the modelled glass melting tank and its system of coordinates.*

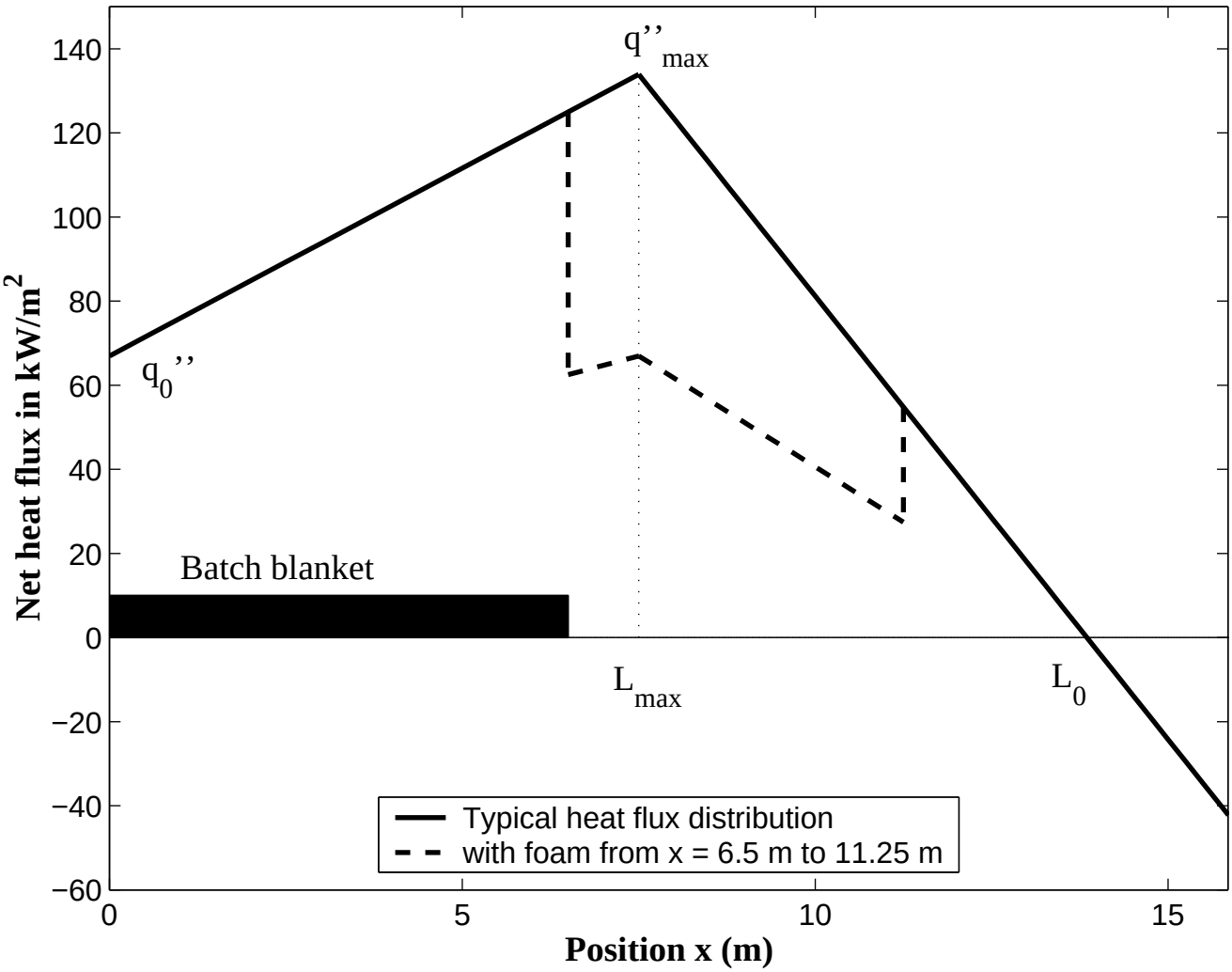


Figure 2: *Heat flux distribution used as the boundary condition at the glass melt/combustion space interface.*

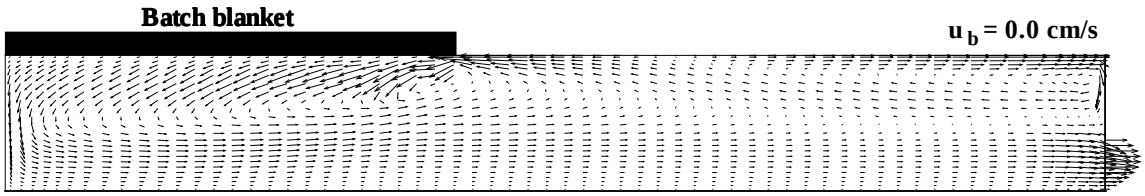


(a)

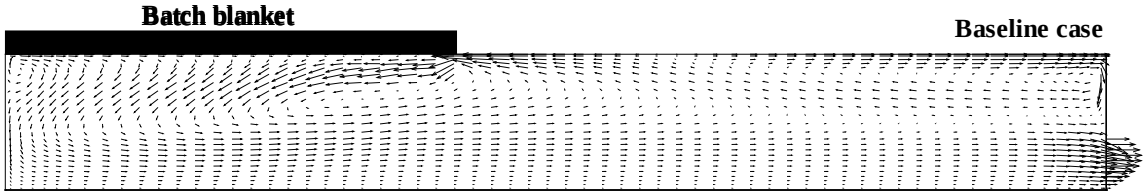


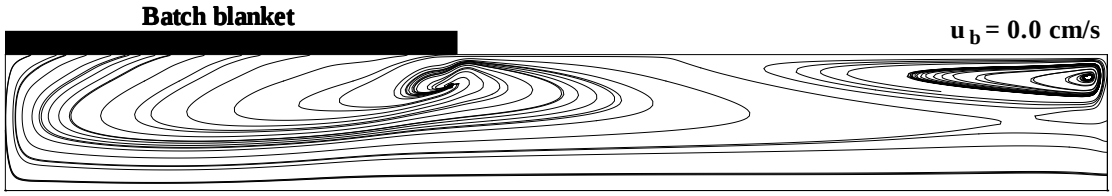


(b)

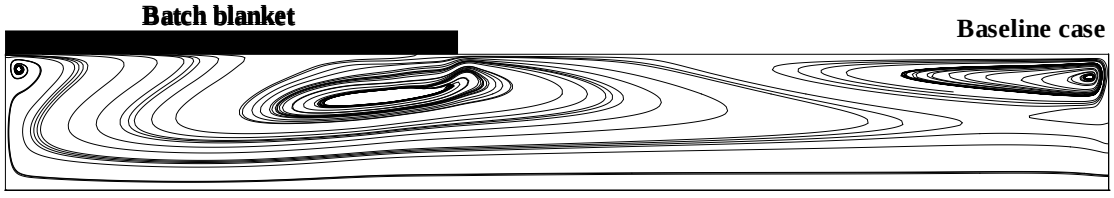


Figure 3: *Effect of the batch velocity on (a) the velocity field, (b) the streamlines at the tank centerline for* $u_{batch}$ *=0.0 cm/s and 0.2 cm/s (baseline case).*

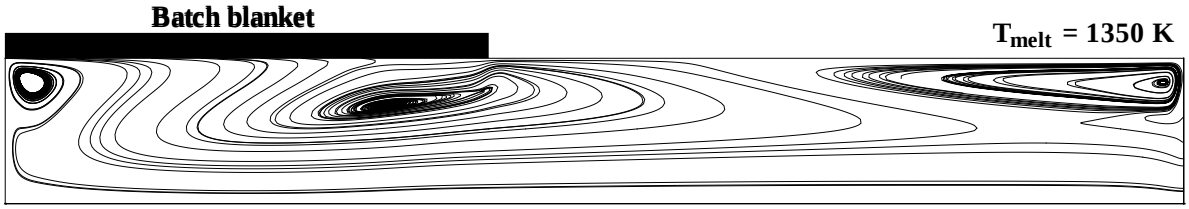


(a)

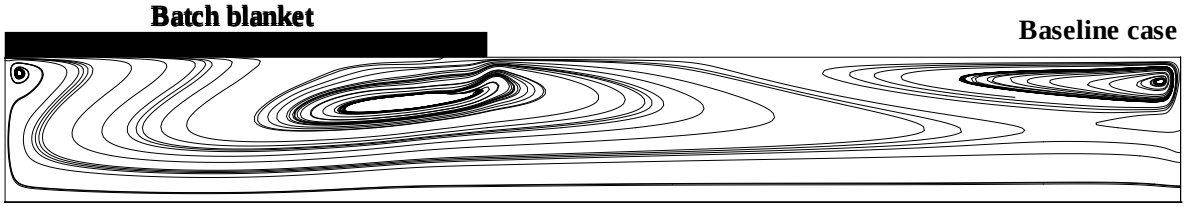


(b)

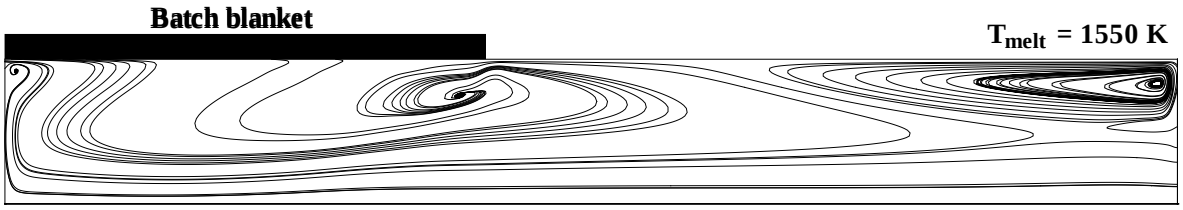


(c)

Figure 4: *Effect of $T_{melt}$ on the streamlines at the centerline for (a) $T_{melt}$ = 1350 K, (b) $T_{melt}$ = 1450 K, (c) $T_{melt}$ = 1550 K.*

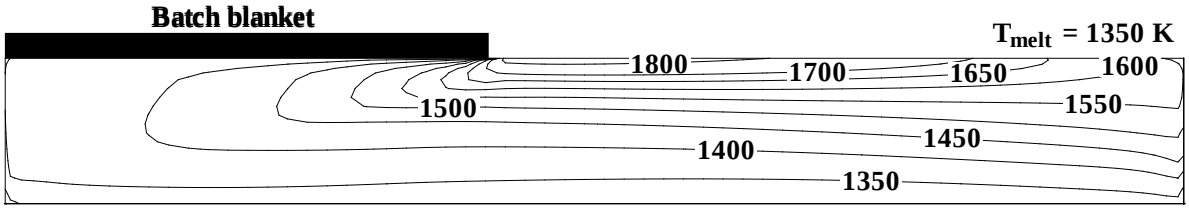


(a)

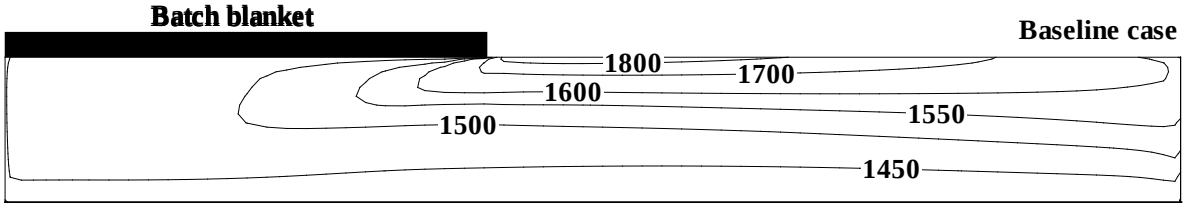


(b)

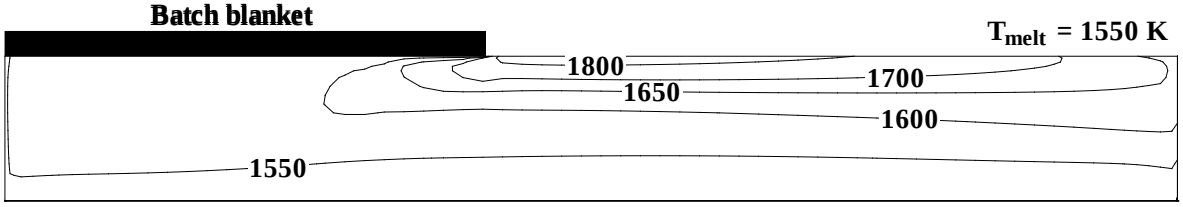


(c)

Figure 5: *Effect of $T_{melt}$ on the temperature field at the centerline for (a) $T_{melt}$ = 1350 K, (b) $T_{melt}$ = 1450 K, (c) $T_{melt}$ = 1550 K.*

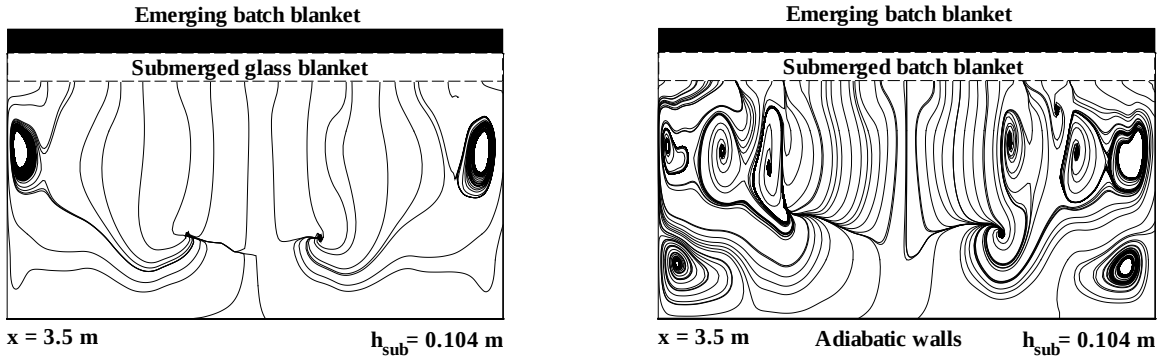


(a)

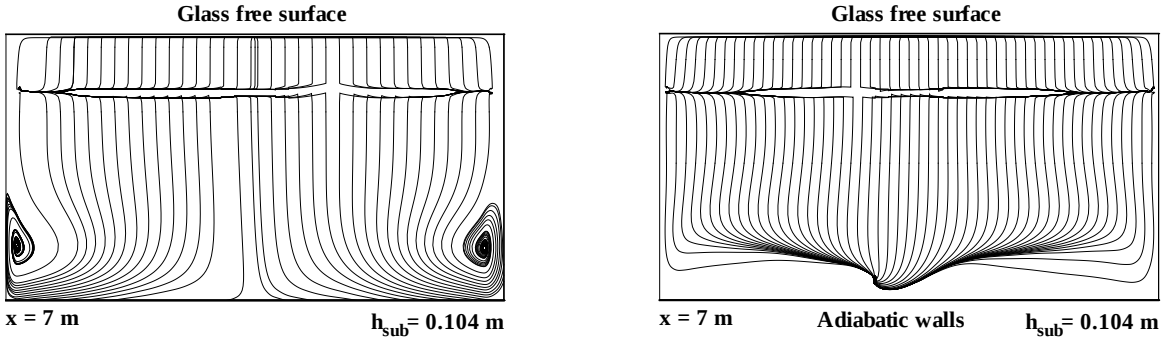


(b)

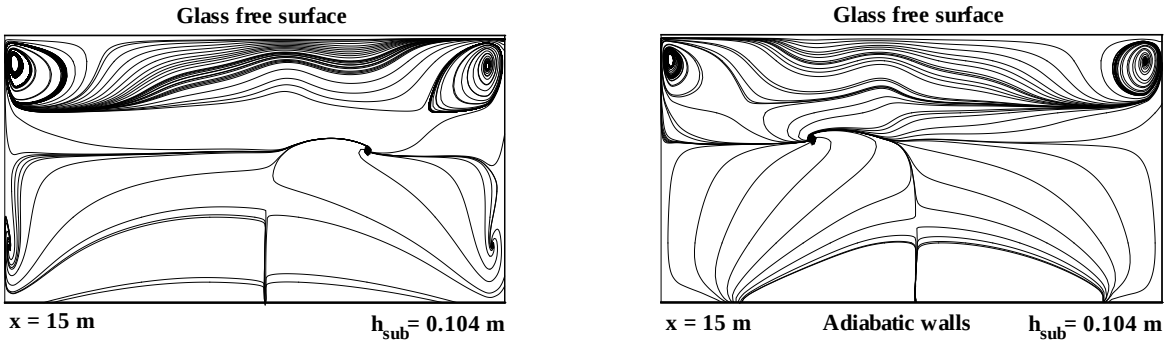


(c)

Figure 6: *Comparison of the streamlines in the spanwise direction at location (a) $x = 3.5$ m, (b) $x = 7$ m, and (c) $x = 15$ m for a 10.4 cm submerged batch with (left) and without (right) heat losses through the side walls.*

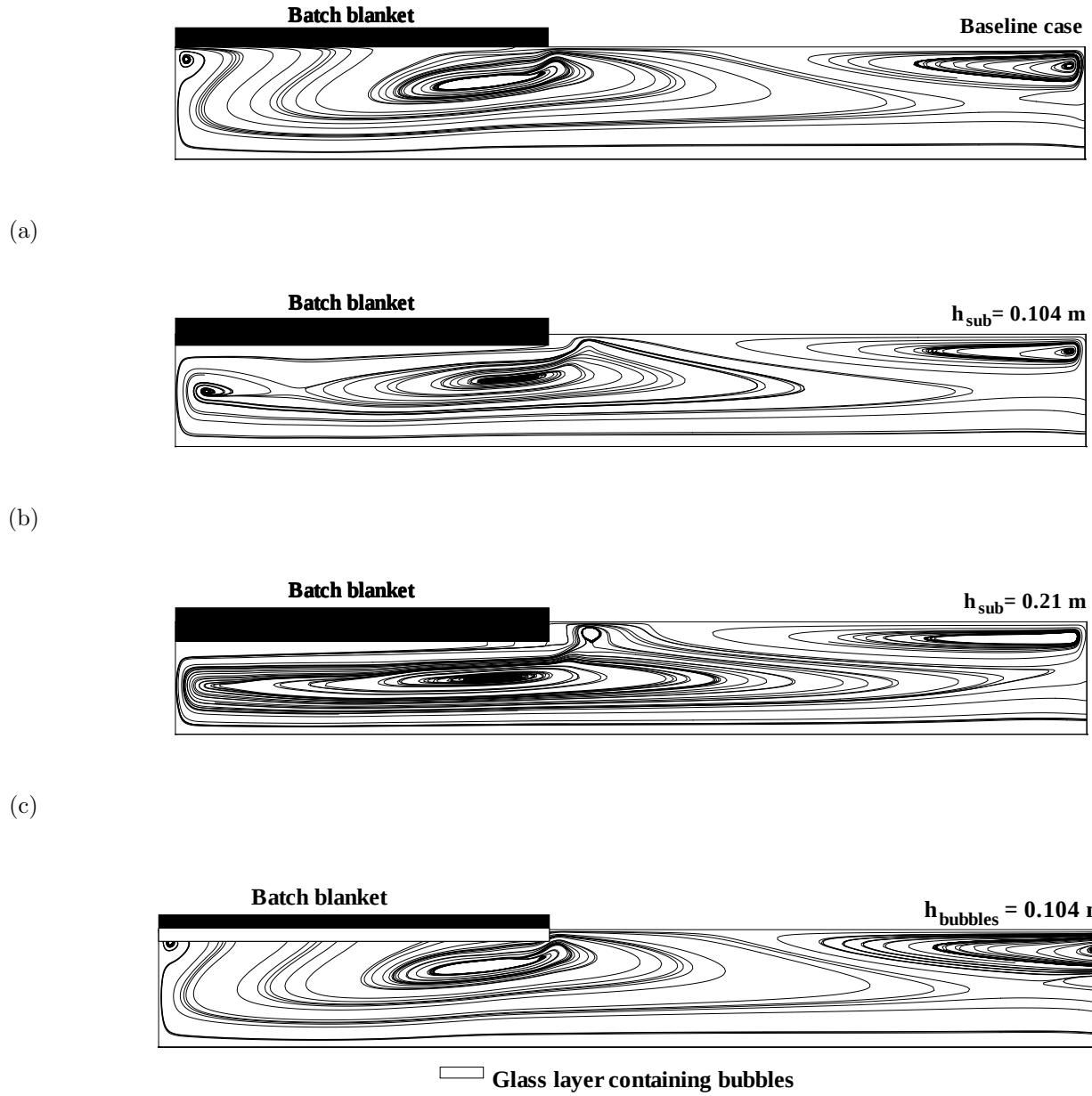


Figure 7: *Effect of the flow reduction under the batch on the streamlines at the centerline for (a) $h_{sub}$=0 m, (b) $h_{sub}$=0.104 m, (c) $h_{sub}$=0.21 m, and (d) $h_{bubbles}$=0.104 m.*

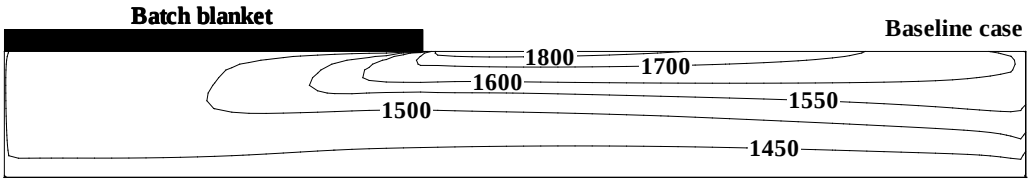


(a)

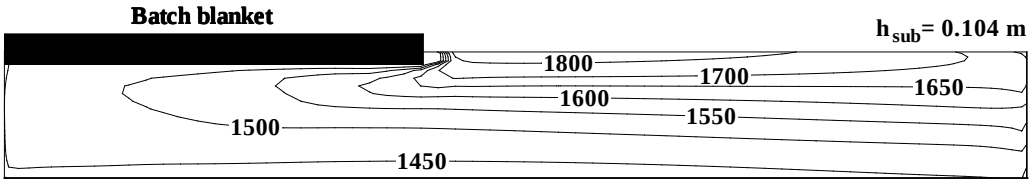


(b)

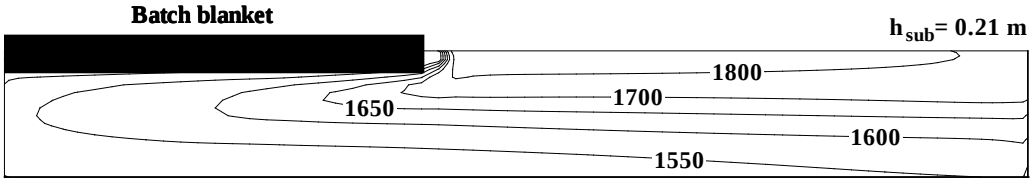


(c)

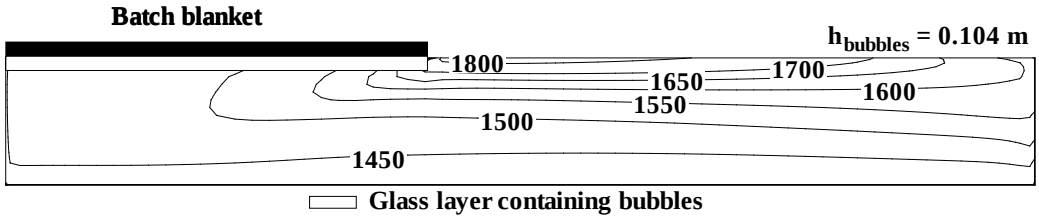


(d)

Figure 8: *Effect of the flow reduction under the batch on the temperature field at the centerline for (a) $h_{sub}$=0 m, (b) $h_{sub}$=0.104 m, (c) $h_{sub}$=0.21 m, and (d) $h_{bubbles}$=0.104 m.*

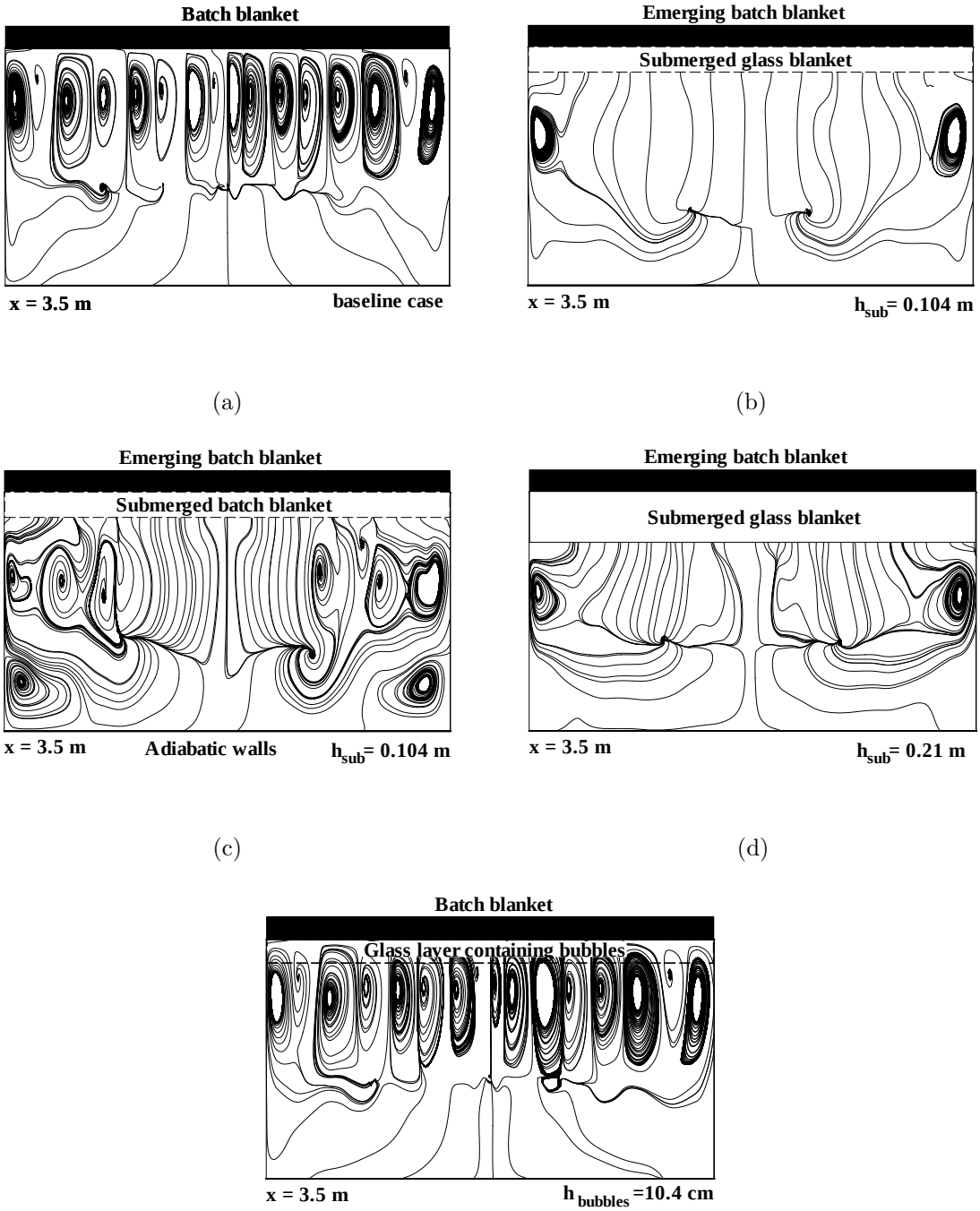


Figure 9: *Effect of the flow reduction under the batch on the streamlines for (a) $h_{sub}$=0 m, (b) $h_{sub}$=0.104 m, (c) $h_{sub}$=0.21 m, (d) $h_{bubbles}$=0.104 m, and (e) adiabatic walls.*

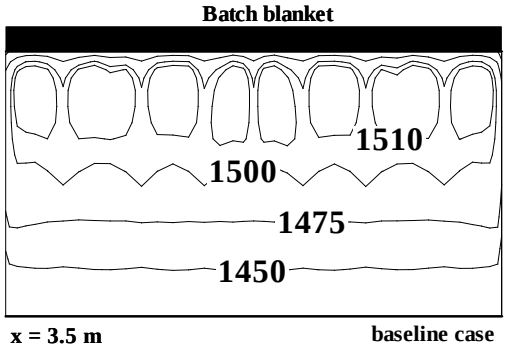


(a)

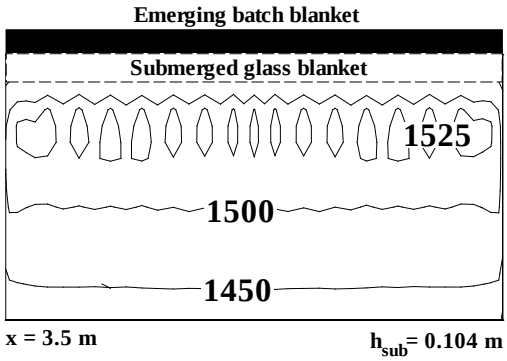


(b)

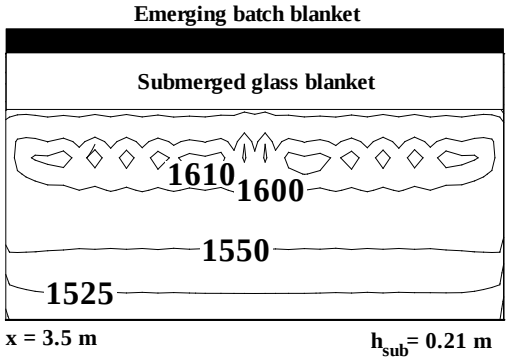


(c)

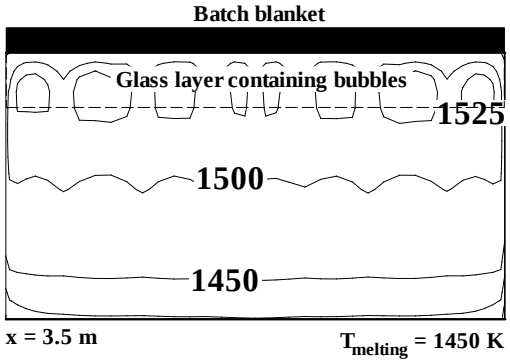


(d)

Figure 10: *Effect of the flow reduction under the batch on the temperature field for (a) $h_{sub}$=0 m, (b) $h_{sub}$=0.104 m, (c) $h_{sub}$=0.21 m, and (d) $h_{bubbles}$=0.104 m.*

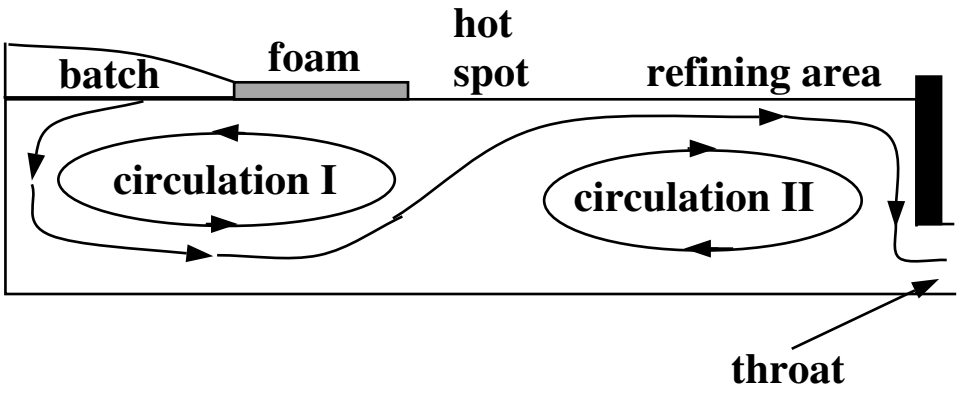


Figure 11: *Schematic of the ideal flow pattern furnaces with a throat.*

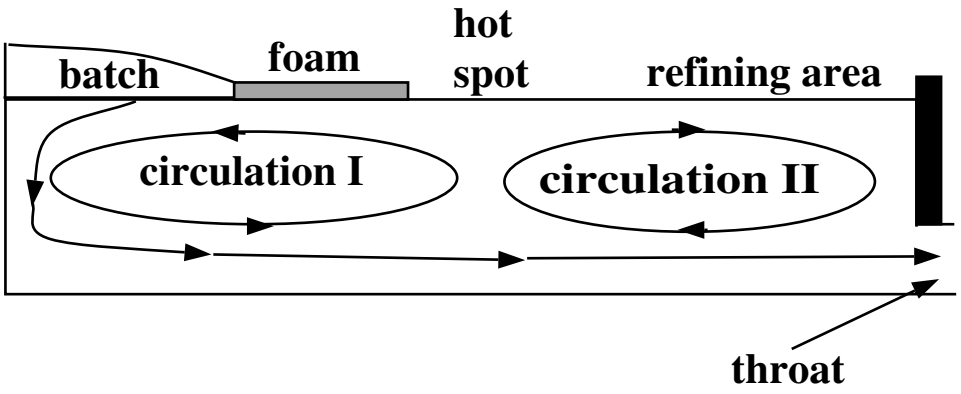


Figure 12: *Schematic of the flow pattern observed by zhiqiang and Zhihao (1997) in furnaces with a throat.*

Table 1: *Summary of the parameters used in the three-dimensional simulation.*

| **Simulation** | $\mathbf{u}_b$ **(m/s)** | $\mathbf{T}_{melt}$ **(K)** | $\mathbf{h}_{sub}$ **(cm)** | $\mathbf{h}_{bubbles}$ **(cm)** | **Gas void fraction** | **Heat losses through walls** |
|---|---|---|---|---|---|---|
| baseline case | 0.2 | 1450 | 0.0 | 0.0 | 0.0 | yes |
| 1 | **0.0** | 1450 | 0.0 | 0.0 | 0.0 | yes |
| 2 | 0.2 | **1350** | 0.0 | 0.0 | 0.0 | yes |
| 3 | 0.2 | **1550** | 0.0 | 0.0 | 0.0 | yes |
| 4 | 0.2 | 1450 | **10.4** | 0.0 | 0.0 | yes |
| 5 | 0.2 | 1450 | **21** | 0.0 | 0.0 | yes |
| 6 | 0.2 | 1450 | 0.0 | **10.4** | **0.2** | yes |
| 7 | 0.2 | 1450 | **10.4** | 0.0 | 0.0 | no (adiabatic) |